JGR Space Physics

RESEARCH ARTICLE
10.1029/2022JA031233

Key Points:

- Clustering Statistics are used to extract large scale turbulence information from 3-m structures in the E-region
- E-region clustering spectra are remarkably similar to in-situ spectra from field-aligned currents in the F-region
- A preferential 5-km scale is simultaneously observed in the E-region and in the F-region field-aligned currents

Correspondence to:
M. F. Ivarsen,
m.f.ivarsen@fys.uio.no

Citation:
Ivarsen, M. F., Lozinsky, A., St-Maurice, J.-P., Spicher, A., Huyghebaert, D., Hussey, G. C., et al. (2023). The distribution of small-scale irregularities in the E-region, and its tendency to match the spectrum of field-aligned current structures in the F-region. *Journal of Geophysical Research: Space Physics*, *128*, e2022JA031233. https://doi.org/10.1029/2022JA031233

Received 13 DEC 2022
Accepted 13 APR 2023

Author Contributions:

Conceptualization: Magnus F. Ivarsen
Data curation: Magnus F. Ivarsen
Formal analysis: Magnus F. Ivarsen, Jean-Pierre St-Maurice, Andres Spicher
Funding acquisition: Jean-Pierre St-Maurice, Glenn C. Hussey
Investigation: Magnus F. Ivarsen, Jean-Pierre St-Maurice, Andres Spicher
Methodology: Magnus F. Ivarsen, Adam Lozinsky
Project Administration: Jean-Pierre St-Maurice, Glenn C. Hussey
Software: Magnus F. Ivarsen, Adam Lozinsky, Devin Huyghebaert, Draven Galeschuk, Brian Pitzel
Supervision: Jean-Pierre St-Maurice, Glenn C. Hussey
Validation: Magnus F. Ivarsen, Adam Lozinsky
Visualization: Magnus F. Ivarsen
Writing – original draft: Magnus F. Ivarsen

The Distribution of Small-Scale Irregularities in the E-Region, and Its Tendency to Match the Spectrum of Field-Aligned Current Structures in the F-Region

Magnus F. Ivarsen[1,2], Adam Lozinsky[1], Jean-Pierre St-Maurice[1,3], Andres Spicher[4], Devin Huyghebaert[4], Glenn C. Hussey[1], Draven Galeschuk[1], Brian Pitzel[1], and Juha Vierinen[4]

[1]Department of Physics and Engineering Physics, University of Saskatchewan, Saskatoon, SK, Canada, [2]Department of Physics, University of Oslo, Oslo, Norway, [3]Department of Physics and Astronomy, University of Western Ontario, London, ON, Canada, [4]Department of Physics, University of Tromsø, Tromsø, Norway

Abstract We associate new data from ICEBEAR, a coherent scatter radar located in Saskatchewan, Canada, with scale-dependent physics in the ionosphere. We subject the large-scale ICEBEAR 3D echo patterns (treated as 2D point clouds) to a data analysis technique hitherto never applied to the ionosphere, a technique that is widely applied in cosmological red-shift surveys to characterize the spatial clustering of galaxies. The technique results in a novel method to calculate the spatial power spectral density of the greater ionospheric irregularity field. We compare results from this method to *in-situ* plasma density and magnetic field observations from the Swarm mission. We show that there is a remarkable similarity between echo clustering spectra in the E-region and the field-aligned current structuring spectrum observed in the F-region: a clear and characteristic preferred scale (5 km) both in the E- and F-region spectra. We discuss the possibility that this represents evidence of an energy injection into the ionospheric irregularity field via energetic particle precipitation, but offer alternative interpretations with wider connotations for the ionosphere-magnetosphere system. These findings open new and promising avenues of research for the study of the location of ionospheric scatter echoes with 3D information. It constitutes a novel way to consider the pattern of ionospheric irregularities over wide fields of view when there is an abundance of radar echoes, which allows for the analysis of radar data as point clouds.

Plain Language Summary With the advent of precision radar data from the aurora containing detailed information about radar echo locations, we are in a position to apply statistical methods from cosmology to extract information about plasma turbulence in the ionosphere. This interdisciplinary paper presents some birds-eye view discussions about the use of correlation functions in physics, showing how it can be used to understand physics on virtually all spatial scales in the observable universe. We present results pertinent to the ionosphere, shedding light on plasma turbulence and its relation to energetic particles in the aurora. Here, we use observations both from space, by the orbiting satellites in the European Space Agency's Swarm mission, and using an experimental auroral radar in Saskatchewan, Canada.

1. Introduction

Plasma instabilities are found on a regular basis in the ionospheric plasma, particularly in elongated forms along the geomagnetic field. In the predominant electrostatic case (fluctuations in the plasma densities in unison with electric field fluctuations) instabilities are triggered for electric fields of the order of 20 mV/m or greater, namely $\boldsymbol{E} \times \boldsymbol{B}$ drifts in excess of or about 400 m/s (e.g., Fejer & Kelley, 1980). Sharp density gradients may also at times modify the instability threshold, mostly in a minor way. At 50 MHz, this would require 500 m gradient scales or shorter while near 10 MHz, gradient scales as large as 20–30 km could affect the instability threshold (St.-Maurice et al., 1994). It remains that when Farley-Buneman waves (FB waves, Farley, 1963; Buneman, 1963) are embedded in gradient-drift waves, the net electric field direction could depart significantly from the background electric field direction, which explains how Type I waves are sometimes seen vertically at the equator, with horizontal wavelengths of the order of a few km associated with the gradient-drift the purely electric field driven waves are embedded into (Kudeki et al., 1982). The unstable electrostatic structures are detected by radars if there is enough wave power in a Fourier component equal to half the radar wavelength in the case of radar back-scattering (these topics are discussed at length in various review papers, notably in the book by Kelley & Heelis, 1989).

Writing – review & editing: Magnus F. Ivarsen, Adam Lozinsky, Jean-Pierre St-Maurice, Andres Spicher, Devin Huyghebaert, Glenn C. Hussey, Juha Vierinen

In the present paper we are concerned with plasma structures with field-perpendicular scale sizes roughly between 1 and 50 km. In the high-latitude ionosphere, a host of plasma instability mechanisms are associated with km-scale plasma structures (Kintner & Seyler, 1985). Frequently evoked, the gradient drift instability depends on density gradients parallel to an ambient electric field, leading to charge separation and the development of polarization electric fields that lead to an $\boldsymbol{E} \times \boldsymbol{B}$-drift that amplifies the initial density gradients (Tsunoda, 1988). Gradient drift instability growth rates favor plasma structuring on the order of ∼1 km (Tsunoda, 1988), though that scale-size is dependent on local plasma physical conditions (Lamarche et al., 2022). In addition, similar disturbances in the auroral region can be caused by flow shear (Horton et al., 1987; Keskinen et al., 1988) and in some cases the current-convective instability (Kintner & Seyler, 1985). Recently, Ivarsen, St-Maurice et al. (2021) found that plasma density spectra in the auroral F-region systematically favor scale sizes between 2 and 20 km for a possible energy injection. Earlier studies connect such injection events to energy dissipation at scale sizes lower than 2–3 km (Keskinen & Huba, 1990). In all, such km-scale irregularities are well-positioned to cause radio scintillations to GNSS applications, which are widespread in the auroral ionosphere (Hong et al., 2020; Prikryl et al., 2015).

In this study we will present a method of investigation into km-scale irregularities in the auroral E-region. To this end, we will use ground-based radar observations from ICEBEAR. The Ionospheric Continuous-wave E region Bistatic Experimental Auroral Radar, is a coherent scatter radar in Saskatchewan, Canada, operating at a frequency of 49.5 MHz (Huyghebaert et al., 2019). The receiver and transmitter locations are separated by ∼240 km. This allows for a continuous wave operation mode. In the Summer of 2019, ICEBEAR was reconfigured to produce a 3D dataset. The reconfiguration entailed improvements in the software processing of the ICEBEAR echoes, and a physical reconfiguration in the positions of the antannas (Galeschuk, 2021; Lozinsky et al., 2022). The result is a radar instrument with unprecedented resolution in altitude and azimuth, allowing for detailed imaging of the E-region plasma irregularity field if the ambient electric field is strong enough in localized regions inside the field-of-view, with the added caveat that we consider each range-Doppler bin to be coming from a single location. The detected echoes from 3-m plasma irregularities from the auroral E-region are continuously recorded by ICEBEAR during its operating times.

Technically, information about plasma structuring on km-scale is not obtainable with a 50 MHz radar, since it is calibrated to detect 3-m FB waves. In the past, however, this fundamental frequency-restriction in other radars has been circumvented several times before. Farley et al. (1981) introduced interferometry to probe a greater plasma velocity field. Recently, Goodwin and Perry (2022) reconstructed the ionospheric irregularity field by combining fixed-altitude multi-point radar measurements with modeled plasma density altitude profiles. In this context, the present study considers individual radar backscatter echoes as two-dimensional *point clouds*. In the Fourier domain, turbulence at 3-m scale is connected to larger-scale turbulence through the nonlinear transfer of energy between wavevectors. The central premise for the present study and the ones mentioned above is then that the spatial distribution of 3-m FB waves trace the greater irregularity field, relations that are revealed by analysis of the spatial correlations present in said distribution. In doing so, we demonstrate the successful application of point clustering statistics adapted from cosmology, the *two point correlation function*. This Monte-Carlo based statistical method appears in cosmology (Ivarsen et al., 2016), fluid mechanics (Falkovich et al., 2001), and particle physics (Verde et al., 2006), to mention a few applications, but has hitherto not been applied to ionospheric observations.

Our motivation comes from Ivarsen et al. (2023), where we demonstrated that ICEBEAR 3D echoes from the ionosphere tend to cluster in time and space. In that paper, empirical metrics of clustering were set up in order to separate ionospheric scatter from meteor trail echoes originating in the upper atmosphere. We showed that the median distance between an ionospheric scatter echo and its 512 nearest neighbors is, on average, 2–5 km, while the corresponding separation for meteor trail echoes were 100–300 km. However, the 512-nearest neighbor distance metric is entirely empirical and without any first-principles basis. In the present report, we show how the clustering of 3-m FB waves can be used to probe plasma turbulence on a wide range of spatial scales.

We analyze radar echoes recorded during four separate events, three of which were seen in conjunction with *in-situ* satellite observations in the F-region from the Swarm mission. For each event, we have obtained ICEBEAR radar echo clustering statistics with the two-point correlation function, from which we estimate the irregularity field power spectral density (PSD). We then proceeded to compare spectra obtained in this way to the PSD of high-resolution magnetic field observations from Swarm, driving us to conclude that the auroral imaging of radar echoes is closely associated with the widespread presence of precipitating particles, at least at times.

2. Methodology

A concept central to the present study is the power spectral density. With this technique one can study the scale-dependent ionospheric irregularity field in both the spatial and temporal domains. As a reference for our methodology, we have included an Appendix that briefly summarizes the foundations of PSD analysis with regard to the topic at hand. Such PSD analyses have been applied to plasma observed by spacecraft with field-perpendicular motion in countless studies (see, e.g., Ivarsen et al., 2019; Ivarsen, Jin, et al., 2021; Kivanç & Heelis, 1998; Mounir et al., 1991; Phelps & Sagalyn, 1976; Spicher et al., 2014; Šafránková et al., 2015; Villain et al., 1986)). Common to most of these space physics studies into the PSD of fluctuating quantities is an interest into spectral slopes. That is, a power law fit of P against ω yields linear curves with a constant slope α (Ivarsen, St-Maurice et al., 2021; Mounir et al., 1991; Phelps & Sagalyn, 1976; Spicher et al., 2014; Tsunoda, 1988),

$$P(\omega) \propto \omega^{-\alpha}, \tag{1}$$

where $\alpha > 0$. In turbulence theory, spectra often display a break-point in $P(\omega)$, the presence of which can indicate a transition to turbulent mixing or energy dissipation (Keskinen & Huba, 1990; Mounir et al., 1991; Tsunoda, 1988), or the presence two-dimensional turbulence (Kintner & Seyler, 1985). A multitude of such break-points has indeed been observed in space plasma (Basu et al., 1990; Ivarsen, St-Maurice et al., 2021; Kelley & Heelis, 1989; Mounir et al., 1991; Spicher et al., 2014; Villain et al., 1986). Importantly, steepening spectra with a second, or steepened, spectral index around $\alpha \sim 3$ are associated with energy dissipation (Ivarsen et al., 2019; Mounir et al., 1991).

Next, we shall introduce a completely novel method to estimate the power spectral density of an ionospheric quantity, the tendency for 3-m FB waves to cluster in the E-region. To explain the method in detail, we must first turn to a different scientific field: statistical cosmology.

2.1. The Two-Point Correlation Function

In cosmology, a common way to quantify the clustering of galaxies and galaxy clusters is the two-point correlation function, $\xi(r)$. Frequently used in large-scale surveys of galaxy redshifts, it is defined as the "excess probability" dp (over random) of finding a galaxy pair separated by a distance r (Davis & Peebles, 1977; Shore & Trimble, 2003). This excess probability is given by

$$dp = n^2[1 + \xi(r)]dV_1 dV_2, \tag{2}$$

where $\xi(r)$ is the two-point correlation function, and where n is the mean number density of galaxies, assumed equal in their respective volume elements, dV_1 and dV_2.

An equivalent approach consists in defining the number density field $\rho(x)$ as a function of a spatial location x, where a spatial averaging would yield $\langle\rho(x)\rangle = n$. Then,

$$n^2[1 + \xi(r)] \equiv \langle\rho(x)\rho(x + r)\rangle. \tag{3}$$

The correlation function $\xi(r)$ can be arbitrarily positive or negative, and goes to zero as the separation r diverges to infinity, assuming a constant average density in the volume. Given the definition, $\xi(r)$ can be thought of as the fluctuating part of the autocorrelation function, meaning that it should be normalized before interpreting its value. Crucially, the correlation function depends only on pair separation distances. This requires the catalog of galaxies to be statistically isotropic and homogeneous. In general, the two-point correlation function is an autocorrelation function (Davis & Peebles, 1977), and is consequently directly related to the power spectrum through a Fourier transform, a fact that we shall exploit in the next section.

2.2. Application to the Ionosphere (the Hankel Transform)

On the very smallest scales, in experimental particle physics, the two-point correlation function is used to model the behavior of charged and neutral particles undergoing collisions (Lisa et al., 1993; Verde et al., 2006). In theoretical plasma physics two-point correlations are formally used to add short range interactions between particles on scales smaller than the Debye length. Much like in other fields, this is done through the use of the cluster expansion scheme based on the so-called BBGKY procedure (Boyd & Sanderson, 1969, Chapter 10). In

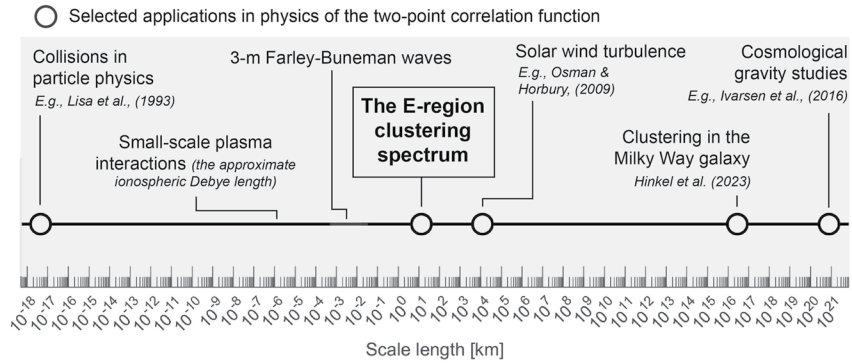

Figure 1. Diagram showing the wide range of spatial scales on which the two-point correlation function has been applied in physics as black circles. The 3-m length scale involved with the FB waves observed in the present study is indicated.

ionospheric physics, correlation functions are used in the theory of incoherent scatter to model plasma density fluctuations on scales larger than the Debye length (Farley, 1969; Hagfors, 1961; Milla & Kudeki, 2011). In the fundamental study of turbulence, hypothetical samples of the fluid velocity field are often treated using two-point correlation methods (Canet et al., 2017; Galtier & Banerjee, 2011). There, it is typically applied to model turbulent behavior in a fluid, with the goal of quantifying the nonlinear transfer of energy between wavenumbers in models and simulations (Falkovich et al., 2001), without the explicit observations of point-sources. Plasma turbulence in the solar wind have been investigated using the observational application of the two-point correlation function, leveraging multi-point observations by several orbiting spacecrafts (Osman & Horbury, 2006, 2009). As we have alluded to, the two-point correlation function is used in cosmology to measure the tendency for matter to cluster in both real and simulated surveys of galaxies and galaxy clusters. In cosmology, the intent is to quantify how gravity works on the largest scales, an important and open question (Bull et al., 2016). Importantly, the cosmological application of the two-point correlation function is observational, and it is applied to the locations of *point sources*. It is this methodology of two-point statistics that we adapt to a point-cloud database of coherent scatter echoes.

Based on the foregoing discussion, we show in Figure 1 a diagram of the various applications of the two-point correlation function in physics. Figure 1 spans almost 40 orders of magnitude, a scale interval that encompasses most of the phenomena found in the observable universe.

Counter to galaxies, ionospheric plasma irregularities are obviously not clustering due to gravitational attraction. E-region plasma irregularities are associated with electric fields, currents, and density gradients, their detection also clearly depends on the ambient plasma density, which is itself driven by energetic precipitation in the nighttime aurora (Huyghebaert et al., 2021). As a result the observed irregularities are detected in clearly delineated regions of abundant structures. This is to say: 3-m structures detected by 50 MHz radars are organized through much larger, 10–100 km patterns in the driving perpendicular electric field and perpendicular density gradients while their very *detection* (not their presence as such) might also be regulated to a large degree by particle precipitation.

We assume here that the scattering layer is thin and essentially flat for the region of interest. The assumption of a thin flat scattering layer is equivalent to saying that we only consider the horizontal (field-perpendicular) distribution of irregularities. We then investigate what would happen in the event of a dominant cylindrical symmetry about a central axis passing through the center of the echo region and by that we mean that we assume *local small-scale isotropy*. We then consider a Fourier transform for this 2-dimensional (2D) cylindrical symmetric situation in which there is no angular dependence in real space nor in **k** space. The 2-D Fourier transform of ρ, which we label as ρ_k, can now be written as

$$\rho_{\mathbf{k}}(k) = \int_0^{\infty} dr \int_0^{2\pi} d\theta dr \rho(r) \exp[ikr\cos(\theta - \phi)] = 2\pi \int_0^{\infty} drr\rho(r) J_0(kr), \tag{4}$$

where subscript **k** indicates a 2-D Fourier transformation. This expression assumes that the density ρ is essentially independent of the position angle θ, while ϕ is the angular position of the wavevector **k** (in k-space cylindrical

coordinates). The final integral, which contains the zeroth order Bessel function of the first kind, $J_0(kr)$, is the Hankel transform. We note that because of the angular symmetry involved in the procedure, the inverse transform has the same form, with ρ_k replacing ρ and k replacing r in the final integral, namely

$$\rho(r) = \frac{1}{2\pi}\int_0^\infty dk k\rho_k(k)J_0(kr) \tag{5}$$

Of course the same expressions apply for $\xi(r)$ and $\xi_k(k)$ since n^2 in Equation 3 is, by definition, a constant. Since $\xi(r)$ is an autocorrelation function (Davis & Peebles, 1977), and based on the foregoing, we are left with (Szapudi et al., 2005),

$$\xi(r) = \frac{1}{2\pi}\int_0^\infty P(k)J_0(kr)\,kdk, \tag{6}$$

the inverse of which implies,

$$P(k) = \int_0^\infty \xi(r)J_0(kr)\,rdr. \tag{7}$$

The above equations constitute the Hankel and inverse Hankel transforms respectively (Baddour, 2011), and are reminiscent of the Wiener-Kinchkin theorem with $\xi(r)$ as an autocorrelation function (see Equation A1, A2).

As already eluded to above, in order to apply the foregoing to ionospheric plasma irregularities seen by a 50 MHz radar, we have to rely on a few basic assumptions. First, we treat echoes as coming from a thin spherical surface above Earth at an altitude close to 105 km, which conforms with the reigning view of the ionospheric location of Farley-Buneman instabilities. Second, we assume that 3-m Farley-Buneman irregularities are sufficiently widespread, to the degree that their distribution is statistically reasonably homogeneous and isotropic, meaning in the present context that on the surveyed surface there is no *local* preferred direction about a central axis of symmetry, though asymmetric dynamics are also captured by the Hankel transform (Baddour, 2011). Third, we assume that the distribution of the echo locations is organized according to a much larger structuring of the E-region plasma, itself the result of arrangement of sources of the small scale irregularities and plasma density enhancements through particle precipitation.

When the above assumptions hold true, we can determine the two-point correlation function $\xi(r)$; that is, the excess probability of finding a 3-m FB irregularity echo pair separated by a distance r on the surface of the E-region as observed by ICEBEAR. We can therefore survey the greater structuring of E-region plasma at some scale r. Consequently, we can obtain a spectrum of irregularity locations by a Hankel transform of the measured $\xi(r)$, whenever the mentioned assumptions are fulfilled to a reasonable degree. Such a spectrum can yield invaluable information about the growth and decay of km-scale turbulent plasma structures (Ivarsen, Jin, et al., 2021), which may lead to detrimental GPS radio scintillations (Kintner P. M. et al., 2007; Prikryl et al., 2015; Yeh & Liu, 1982).

2.3. ICEBEAR 3D Data

The ICEBEAR 3D dataproduct provide the echo locations (latitude, longitude, and altitude) of the Doppler shift and signal-to-noise ratio (SNR) of individual scattering targets. As outlined above, we consider all echoes to originate from a thin layer (a surface in that sense) located 105 km above Earth's surface, though the exact altitude of this layer has little impact on the results of the present study. The ICEBEAR 3D dataset allows for roughly 1.5 km as the smallest spatial separation, with a temporal cadence of 1 s. For each echo population considered, only the position in latitude and longitude are considered, and we apply a signal-to-noise ratio (SNR) cut-off of 2 dB to avoid noisy echoes. After the data preparation procedure, the spatial echo locations are used to calculate the two-point correlation function for a given echo population.

To estimate $\xi(r)$, we apply the Landy-Szalay estimator for the two-point correlation function (Ivarsen et al., 2016; Kerscher et al., 2000; Landy & Szalay, 1993), which is written as

$$\xi(r) = \frac{DD(r) - 2DR(r) + RR(r)}{RR}. \tag{8}$$

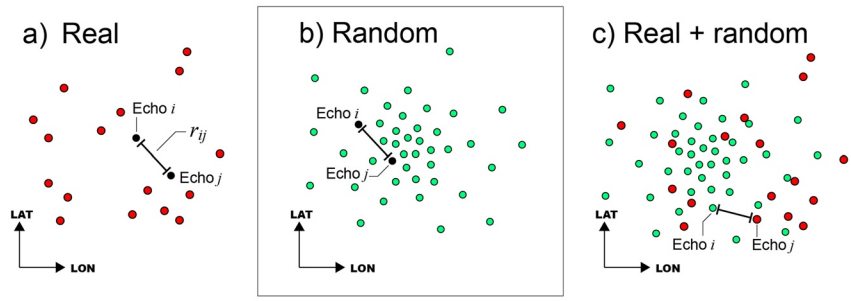

Figure 2. A schematic illustration of the Landy-Szalay estimator for the two-point correlation function. Panel (a) shows a real point distribution, panel (b) shows a random point distribution, while panel (c) shows the two distributions superposed. In panel (a), real pair separations are calculated, while random pair separations are calculated in panel (b). In panel (c), pair separations between real and random pairs are counted.

In this expression, $RR(r)$ is the number of "random-random" echo pairs separated by a distance r. Likewise, $DR(r)$ and $DD(r)$ are "random-real" and "real-rea" pairs respectively. The usage of Random locations means that we are in effect estimating $\xi(r)$ using a Monte Carlo simulation that is based on a random Poisson distribution in the same spatial volume that is inhabited by the real echoes (with a suitable standard deviation). Those "real echoes" refer to the population of E-region echoes that is actually observed by ICEBEAR 3D. Each pair count is normalized, that is to say:

$$DD(r) = \frac{dd(r)}{n_d(n_d-1)/2}, \quad RR(r) = \frac{rr(r)}{n_r(n_r-1)/2} \quad \text{and} \quad DR(r) = \frac{dr(r)}{n_d n_r}, \tag{9}$$

Here, $dd(r)$, $rr(r)$ and $dr(r)$ are the absolute pair counts, and n_d and n_r are the total number of real and random echoes respectively. Figure 2 illustrates the process; real points (red) and random points (green) are treated separately (panels a and b), and in superposition (panel c).

After applying the estimator Equation 8 to a population of echoes, we apply a Hankel transformation to $\xi(r)$ to evaluate Equation 7. Special care must be taken when evaluating this integral, as the Bessel functions can oscillate rapidly around zero. We follow the method outlined in Guizar-Sicairos and Gutiérrez-Vega (2004), where we interpolate the function $\xi(r)$ at the Bessel function roots in order to a priori estimate the Bessel function integral, akin to a Gaussian quadrature method. Here we note that the parameter n_r (the number of random points to use in the Monte Carlo simulation) is not crucial as long as n_r is high enough that there is a reasonable number of random echo pairs at each separation at which we find real echo pairs. If n_r is not high enough, however, $\xi(r)$ will not converge toward zero at infinity, which strongly interferes with the numerical integration of Equation 7. We use $n_r = 3n_d$, which we find to be adequate without taking up too many computing resources.

2.4. The Rayleigh Criterion

The ICEBEAR 3D processing can produce a full field of view image for every range-Doppler time bin, at a rate of 200,000 images per second. In each image, multiple targets may exist and be uniquely identifiable provided the targets are spatially separated by distances greater than the Rayleigh criterion limit which is ~25 km. A selection algorithm locates the azimuth and elevation angle of arrival of only the strongest source. In order to obtain an azimuthal spatial resolution of 1.5 km, ICEBEAR 3D processing then makes the assumption that it is rare for more than one target to occur at the same range, with the same Doppler frequency, in the same second. In other words, ICEBEAR 3D's operating principles assume each echo comes from a single volume with a single peak in SNR, where this peak location is determined through interferometry, thereby circumventing the Rayleigh Criterion.

3. Results

We have applied the new methodology to populations of ICEBEAR 3D coherent scatter echoes, and we will now go over a few representative events. For each of the events we present, ICEBEAR records a very high number of echoes in a relatively short duration of time (1 min), meaning that the conditions are ideal for the application of the two-point correlation function: the relatively short time scale means (as we checked) that the ionospheric

conditions were not changing drastically while the very large number of echoes means that a relatively large survey volume was being sampled.

In Figure 3 we show two example echo populations and their corresponding clustering power spectral density. In panels a–c) we present a population of 36,000 echoes recorded during the 1-min interval between 05:42 UT and 05:43 UT on 21 February 2021, while panels d–f) present the next 1-min interval from 05:43 UT to 05:44 UT. Panels a) and d) show echo signal-to-noise ratio (SNR) while panels b) and e) show echo Doppler velocity, both binned by magnetic latitude and magnetic longitude, using the altitude adjusted corrected geomagnetic coordinate system (Baker & Wing, 1989). In panels (c) and (f) we show the two-point correlation function $\xi(r)$ for the two populations, using the estimator given in Equation 8. In panel (g) we show the Hankel transform of $\xi(r)$ (the clustering power spectral density) for both the foregoing populations, with the overall spectral index indicated. The two spectra are normalized so that their integrated value (root-mean-square) equals the median SNR value for the two populations.

We see that whereas the two events show Doppler velocities centered narrowly around 350 m/s, they exhibit rich structure in SNR, highlighting how the echoes trace the greater structure of the auroral E-region ionosphere. From considering that the two populations are situated in the same volume of geomagnetic space, we can make some deductions about the temporal evolution of the ionospheric irregularity field there. First we note that the whole echo structure appears to move roughly one degree longitude in the westward direction (an approximately 45 km distance). Given 60 s, this constitutes an apparent echo bulk velocity of 750 m/s westward motion. The next observation we make is that the recorded number of echoes go from 36,000 to 20,000, a considerable reduction. At the same time, it seems that a large part of the large-scale high-SNR structuring is missing in the second interval, indicating widespread dissipation in the irregularity field during the second interval. We will now go through the shapewise difference from the first population to the next. Spectrum II steepens somewhat on scales larger than ∼10 km. While spectrum I already shallows slightly for scales smaller than 10 km, there is in spectrum II a clear power enhancement at those scales (∼6 km). An overall spectral slope of −2.6 accurately describes the overall decay in power for both spectra, despite the small-scale enhancements. This is to say that the observed temporal evolution introduces changes in power on all scales, indicating a highly dynamical system, but that the overall spectral shapes nevertheless remain broadly similar.

The large well-defined peak at ∼6 km in spectrum II is reflected in $\xi(r)$ (panel f). Going back to the definition of the two-point correlation function, this enhancement in ξ indicates a higher probability (compared to random) of finding echo pairs at these separations, and in terms of power spectral density the bumps can indicate an energy injection on those scales. However, the apparent reduction in power in the wavevectors surrounding the 5 km peak in panel g) is reminiscent of clustering in the real sense, and not an injection of energy.

The clustering spectra in Figure 3 show abundant useful information about the clustering of 3-m FB waves in the auroral E-region on scales between 1.5 and 75 km. However, there is a need to directly associate the clustering spectrum to an established metric of turbulence in the ionosphere. To this end, we present three conjunctions between satellites from the European Space Agency (ESA) and ICEBEAR, beginning with an especially auspicious conjunction on 28 August 2021, between ICEBEAR and Swarm B. The satellite Swarm B is one of three satellites in the ESA's Swarm mission (Friis-Christensen et al., 2006). Swarm B orbits Earth at an altitude of around 500 km in the F-region ionosphere, carrying a host of scientific instruments. Since we need information about km-scale plasma turbulence, we use 50 Hz B-field data from the on-board Vector Field Magnetometer, along with 2 Hz plasma density measurements from Swarm's Langmuir probe (there is no data from the advanced 16 Hz Plasma Density dataset for these conjunctions). To obtain perpendicular magnetic field data, whose fluctuations are associated with the field-aligned currents (FAC) caused by precipitating electrons, we transform the residual B-field vectors into the Mean Field Aligned (MFA) coordinate system. The MFA coordinate system has one component parallel to the mean-field (z), one pointing in geomagnetic east (y), with the third component completing the triad (meridional, x) (Ivarsen et al., 2020; Park et al., 2017).

Figure 4 shows a conjunction between Swarm B and ICEBEAR at 06:45 UT on 28 August 2021, when ICEBEAR made continuous observations of echoes at two locations near Swarm B's orbit. We use 2 minutes of satellite observations. Panel a) shows the SNR of 22,000 echoes binned by magnetic longitude and latitude, with Swarm B's southward orbit shown by the red line. Panel b) shows the satellite's 2 Hz plasma density observations in the two-minute interval of the conjunction, while the corresponding density spectrum is shown in panel c). Here, the x-axis shows temporal frequencies, while the top x-axis shows the corresponding spatial scale, assuming that

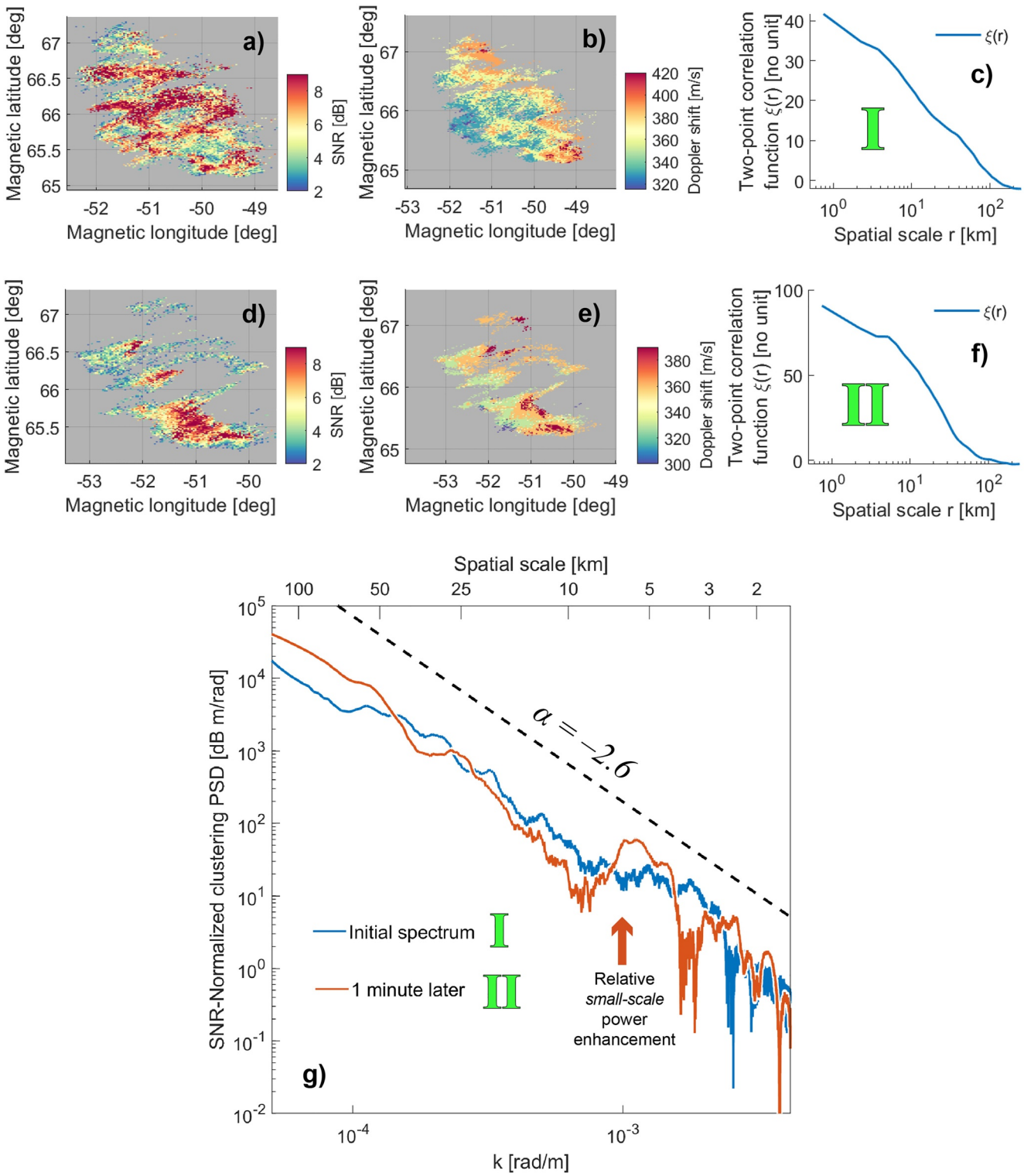

Figure 3. Clustering statistics for two example echo populations. Panels (a)–(c) show an event during which 36,000 echoes were recorded between 05:42 UT and 05:43 UT on 21 February 2021, whereas panels (d)–(f) show 20,000 echoes recorded in the subsequent minute, between 05:43 UT and 05:44 UT. Panels (a) and (d) show SNR, while panels (b) and (e) show echo Doppler velocity, both binned by magnetic latitude and longitude. Panels (c) and (f) show the two-point correlation function $\xi(r)$ resulting from correlating echo pairs in both spatial distributions. Panel (g) shows the Hankel transform of $\xi(r)$ for the two events, with Roman numeral indicating which is which. The lower x-axis shows wavenumber k while the upper x-axis shows spatial scale r, and the overall spectral slope (α) for both spectra is shown by the black dashed line. An orange arrow indicates a relative small-scale power enhancement in spectrum II compared to spectrum (i).

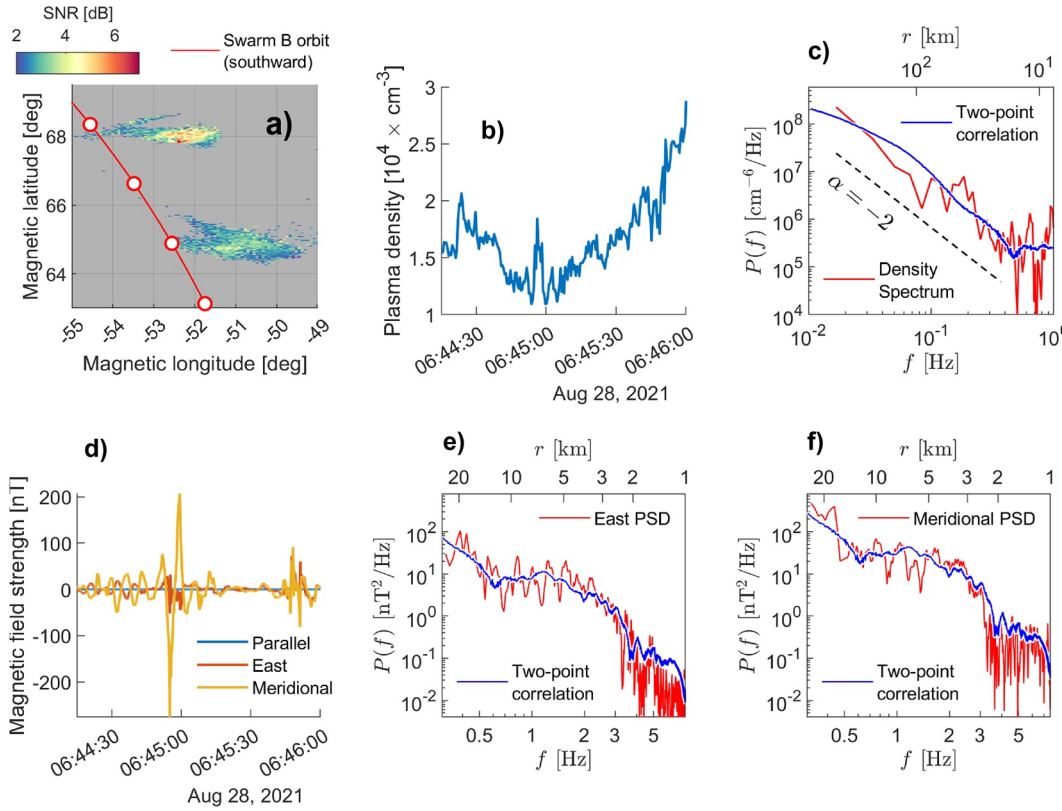

Figure 4. A conjunction between Swarm B and ICEBEAR at around 06:45 UT on 28 August 2021. Panel (a) shows echo SNR binned by magnetic longitude and latitude, and Swarm B's descending orbit by the red line, where the red circles in panel (a) correspond to the *x*-axis tickmarks in panels (b) and (d). Panel (b) shows the Swarm-measured 2 Hz plasma density. Panel (c) shows the density spectrum based on the measurements in panel (b) by the red line, while the composite Hankel transform of ICEBEAR echo locations during the conjunction is shown in blue line. A dashed black line indicates the spectral slope of −2. Panel (d) shows the Swarm-measured high-resolution (50 Hz) residual magnetic field fluctuations in the MFA reference frame. Panels (e) and (f) show the PSD of the two field-perpendicular components by the red line, and the composite Hankel-transformed two-point correlation function by the blue line. In panels (c), (e) and (f), the ICEBEAR spectra are normalized to the same RMS as the Swarm spectra. The temporal sampling frequency is shown in Hz on the bottom *x*-axes (corresponding to the Swarm measurements), while the corresponding spatial scale is shown on the top *x*-axis.

the local plasma velocity is negligible compared to Swarm B's orbital velocity (7,600 m/s). We overplot in blue line a composite clustering spectrum from ICEBEAR, normalized to the same RMS as the density spectrum. (During the two-minute interval, ICEBEAR observed two distinct echo populations, and so we calculated a total of four 1-min clustering spectra. The blue line shows the mean spectrum based on all four spectra.)

Panel d) of Figure 4 shows Swarm B's 50 Hz magnetic field observations in the MFA frame from the mentioned two-minute interval, exhibiting significant fluctuations reaching 200 nT. Panels e) and f) show the PSD of the east (e) and meridional (f) components in thin red line, for spatial scales between 25 and 1 km—the large-scale FAC fluctuations are hard to investigate with the current MFA coordinate transformation. Note that although the high-resolution magnetic field observations nominally are associated with a Nyquist scale of 300 m we cut the spectrum off at 1 km. The ICEBEAR clustering spectrum is again overplotted in blue line. For both the density spectrum and the perpendicular magnetic field spectra we use Welch's method of averaged periodograms (Welch, 1967).

To complement the conjunction in Figure 4 we present in Figure 5 two additional conjunctions, this time between ICEBEAR and Swarm A, on 19 April 2021 (upper six panels) and on 4 November 2021 (lower six panels), where we likewise use two minutes of satellite observations. Each panel's layout corresponds to Figure 4 and we refer to that Figure for description. The three conjunctions show consistency in some key aspects. First, the bulk of the echoes occur in areas not associated with strong FAC fluctuations (panel j of Figure 5 is an especially telling example of

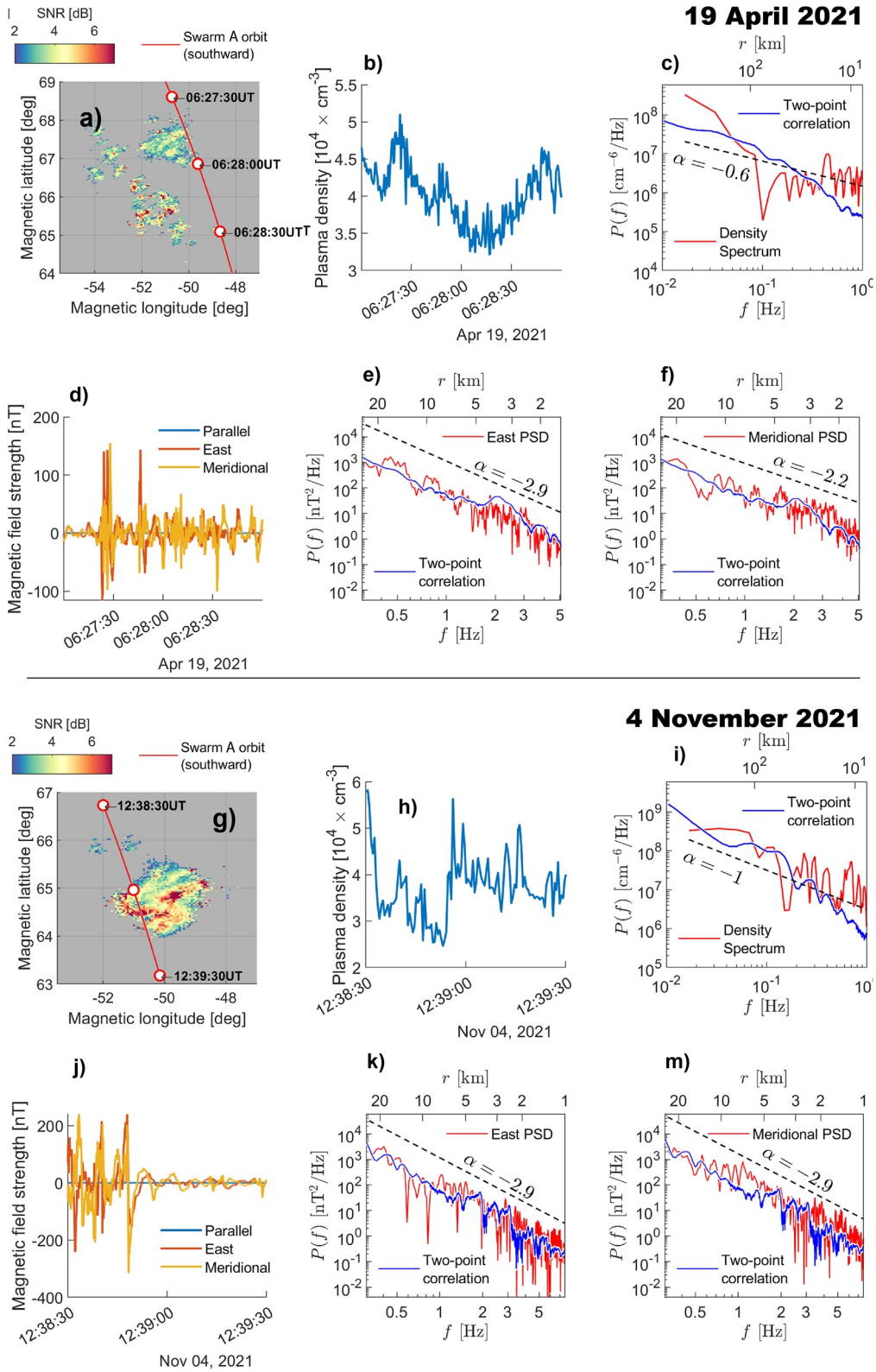

Figure 5. Two additional conjunctions between Swarm satellites and ICEBEAR, on 19 April 2021 (upper six panels) and on 4 November 2021 (lower six panels). See Figure 4 for description.

this behavior: the echoes are positioned just outside the large FAC fluctuations). Nevertheless, all three conjunctions show that small-scale power decay in a similar fashion, with consistent small-scale spectral slopes (panels e, f, k, m of Figure 5). Whereas the large-scale density spectrum in Figure 4 matches that of the clustering spectrum, the agreement does not carry into the two conjunctions shown in Figure 5, where the clustering spectra are consistently steeper than the density spectra. However, the density observations have a sampling frequency of 2 Hz and so only 120 datapoints enter into the PSD analysis—resulting in considerably noisy spectra. The small-scale FAC structuring spectra, though, are based on 6000 observations during two minutes, and so make for stronger statistics. Lastly, we note that the vertical (field-aligned) wavelength of density irregularities observed in the F-region at field-perpendicular scales larger than 1 km maps to E-region altitudes (Ivarsen, St-Maurice et al., 2021), facilitating a comparison of the spectra.

4. Discussion

The sparsely sampled F-region density observations notwithstanding, we observe an overall good agreement between the shape of the B field fluctuations and the ICEBEAR 3D clustering spectra in all three conjunctions. In panels e) and f) (and to a limited extent in panel c) of Figure 4, we see that all spectra exhibit a kink around 15 km: the FAC structuring spectrum, the density spectrum (to a lesser degree), and the clustering spectrum all show a leveling off in the power as a function of frequency near 0.5 Hz, which translates into 15 km scale in space. In panels e) and f), this leveling off is followed by a wide bump centered on 5 km. In other words, for the conjunction shown in Figure 4, small-scale perpendicular magnetic field fluctuations in the F-region and the clustering of 3-m FB waves in the E-region exhibit excellent shape-wise correspondence.

The field-perpendicular magnetic fluctuations correspond to FAC fluctuations, which are in turn related to energetic particles in the aurora, assuming that the FACs are driven by particle precipitation. The implications are that structured FAC patterns have an immediate link with the irregularities seen in the ionospheric E-region. We observe this link directly on kilometer-scale sizes, but it does not follow that the radar-observed 3-m FB waves are similarly linked to FAC structures. Rather, the irregularity echoes may simply trace the km-structures in question, which links with the 3-m FB waves through turbulent cascade or dissipation. Indeed, the spectral steepening that starts at 3 km is particularly interesting. Seen in context with the enhancement in the 15 and 5 km, it could conceivably indicate turbulent dissipation on some *smaller* scales as a consequence of an energy injection on some *larger* scale, as first derived by Kolmogorov (1941). Waves created by the gradient drift instability comes to mind as possible causes of this 5 km -enhancement (Tsunoda, 1988). A more conservative interpretation holds that there simply is a preferred size to field-aligned tubes of precipitation, reflected both in the E-region irregularity distribution organized around those tubes, and in the FACs.

This stated, the timestamps of the FAC fluctuation data reveal that while the prominent spikes in the perpendicular field strength coincide with enhancements in the observed densities, they consistently occur *outside* the region of observed ICEBEAR 3D echo populations. This could be explained in terms of recent findings that the conductivity enhancements associated with precipitation events short-circuits the electric field locally, thereby ultimately suppressing the trigger of irregularities that can be observed by ICEBEAR (Huyghebaert et al., 2021). This reasoning resonates with recent *in-situ* observations from the cusp region (Spicher et al., 2022), aligned with existing viewpoints that predict reduced electric fields in the centers of precipitation regions (Aikio et al., 2002; Maynard et al., 1973).

Our last paragraph brings an interesting question to the fore, namely: why are the FAC structuring spectra in such good agreement with echo clustering spectra when the radar echo regions are outside the region of FAC observations? Irregularity suppression mechanisms can be identified, but why is it that outside the region of precipitation we see plasma echoes with a PSD structure that is basically identical to the FAC PSD? One very tentative answer could be that while the electric field may be too weak in the center of a precipitation region, its pattern outside that precipitation region would match that of the precipitation field. That is to say: as one moves away from the center of charge, the field becomes stronger and plasma instabilities triggered by Hall currents are introduced. But the electric field pattern would still match the source pattern, that is, the shape of the precipitation field in directions perpendicular to the magnetic field. An explanation in the context of recent work by Dimant et al. (2021) involves high-energy electrons. Increases in high-energy electron precipitation should normally be accompanied by conductivity enhancements brought about by the turbulence created by charge deposition at impact altitudes near 120 km. If those conductivity enhancements are suppressed, the action of the precipitating electrons would

cause strong electric field modulations. These electric field modulations could cause density structures and pressure gradients that in turn drive small-scale structuring in the FAC (Laundal et al., 2019).

5. Conclusion

In this study, we have scrutinized the tendency for coherent scatter echoes from ICEBEAR 3D to cluster in space, with completely novel adaptations of techniques used in cosmological galaxy surveys. We demonstrate, through auspicious conjunctions with satellite observations from ESA's Swarm mission, that the two-point correlation function can indeed be used to estimate the power spectral density of the greater irregularity field in the auroral ionosphere. Since each ICEBEAR 3D echo corresponds to a 3-m Farley-Buneman wave, we are relating the apparent clustering of meter-scale irregularities to the ionosphere's greater plasma irregularity field through the nonlinear distribution of turbulent energy.

A remarkable result of the present study is the observation of a turbulent irregularity field simultaneously in the E- and F-region. *The clustering spectrum of* 3-m FB *waves in the E-region matches the FAC structuring spectrum in the F-region*. Both Figures 3 and 4 show clear evidence for a preferred clustering scale at around 5 km, and in an auspicious conjunction with the Swarm B satellite this preferred clustering scale is also found in the FAC structuring. While this preferred clustering scale could conceivably be interpreted in terms of an energy injection, it can also form the basis of investigations into what factors are driving the ionosphere-magnetosphere interaction.

The technique we propose is potentially widely applicable and useful, and opens up new avenues of study into the greater ionospheric plasma irregularity field and the vertical coupling between the E- and F-regions. The present study includes only an initial presentation, and we suggest that future studies into the spatial correlation between coherent scatter radar echoes include analysis of cylindrical symmetries and the general isotropy in the distribution of echoes.

Appendix A: Mathematical Treatment of the *In-Situ* Power Density Spectrum

In the time domain, for a function $n(t)$, the PSD $P(\omega)$ of that time series reflects to what degree that function fluctuates at an angular frequency $\omega = 2\pi/t$. Entirely analogous, in the spatial domain, a fluctuating function $n(r)$ has a characteristic PSD $P(k)$ which reflects the intensity of fluctuations at a wavenumber $k = 2\pi/r$. In both cases, given a weakly stationary function, its PSD is expressible as a Fourier transform of the original fluctuating function's autocorrelation function. That is to say.

$$P(\omega) = \frac{1}{2\pi}\int_{-\infty}^{\infty} d\tau\, R(\tau)e^{-i\omega\tau} \quad \text{for the temporal domain, and} \tag{A1}$$

$$P(k) = \frac{1}{2\pi}\int_{-\infty}^{\infty} dr\, R(r)e^{-ikr} \quad \text{for the spatial domain,} \tag{A2}$$

where R is the autocorrelation function, for relative displacements in time (τ) and space (r). Considering the density field $n(t)$ as samples of a stochastic process, the autocorrelation function is defined using the product between readings separated in time by a shift τ (Ochi, 1998),

$$R(\tau) = \int_{-\infty}^{\infty} dt\, n(t)n(t+\tau), \tag{A3}$$

and similarly for the spatial domain. The fact that rockets and satellites rapidly sample plasma in a volume of space means that a *time series* $n(t)$ can be directly related to the spatial fluctuations in the sample volume, given that the local plasma velocity is much smaller than the velocity of the spacecraft moving through that plasma. In other words, for this particular situation $P(\omega)$ (Equation A1) measures *spatial* fluctuations on a scale r through,

$$r = \frac{2\pi v_s}{\omega}, \tag{A4}$$

where v_s is the velocity of the spacecraft with respect to the plasma being sampled.

A1. Relation Between *In-Situ* Spectra and E-Region Clustering Spectra

We see the need to address the dimensionality of the quantities being compared in Figures 4 and 5, and also explicitly formulate the relation between *in-situ* observations with the two-point correlation function. After all, an orbiting satellite measures a 1D slice through the ionospheric irregularity field (Equation A1), while ICEBEAR clustering spectra from the Hankel transform stem from a 2D point cloud (Equation A2 via Equation 7). Formally, we can relate the methodology presented in Section 2.2 to a spectrum of large scale irregularities obtained along a straight line passing through the axis of symmetry of the system. Let $x = r\cos\theta$ be the value of the spatial coordinate in that case. The PSD $P(k_x)$ has to be given by

$$P(k_x) = \xi_{k_x} = \int_0^{\infty} dr \int_{-\pi/2}^{\pi/2} d\theta r\xi(r)\exp[ik_x r\cos(\theta)], \tag{A5}$$

which conforms to Equation 7:

$$P(k_x) = \pi \int_0^{\infty} drr\xi(r)J_0(k_x r). \tag{A6}$$

This simple factor of 2 difference with the full Hankel transform (Equation 7) result is due to the symmetry property $J_0(\beta) = J_0(-\beta)$. In other words, there is a clear linear relationship between a 1D spectrum resulting from the satellite overpass and the two-dimensional distribution of irregularities. This requires axisymmetry up to a large enough scale, which may be of the order of 100 km, given the excellent agreement in Figures 4e and 4f on scales less than 50 km in size. The close correspondence between the *in-situ* and the ground-based spectra in Figures 4 and 5 should then also be considered in the context of the efficacy of space-based 1D-slice power spectra calculated using Equation A1 (see Fredricks & Coroniti, 1976).

Data Availability Statement

ICEBEAR 3D echo data for 2020, 2021 is published with DOI 10.5281/zenodo.7509022. Data from the European Space Agency's Swarm mission can be downloaded from the webpage https://swarm-diss.eo.esa.int/.

Acknowledgments
We acknowledge the support of the Canadian Space Agency (CSA) [20SUGOICEB; 21SUSTIERI], the Canada Foundation for Innovation (CFI) John R. Evans Leaders Fund [32117] and the Province of Saskatchewan. We also acknowledge the support of the Natural Science and Engineering Research Council (NSERC) and the programs: the International Space Mission Training Program supported by the Collaborative Research and Training Experience (CREATE) [479771-2016] program and the Discovery grants program [RGPIN-2019-19135]; and the Digital Research Alliance of Canada [RRG-FT2109]. AS acknowledges funding from the Research Council of Norway Grant 326039. DH and AS acknowledge UiT The Arctic University of Norway contribution to the EISCAT 3D project funded by the Research Council of Norway - Grant 245683.

References

Aikio, A. T., Lakkala, T., Kozlovsky, A., & Williams, P. J. S. (2002). Electric fields and currents of stable drifting auroral arcs in the evening sector. *Journal of Geophysical Research*, *107*(A12), SIA31–14. https://doi.org/10.1029/2001JA009172

Baddour, N. (2011). Chapter 1 - two-dimensional Fourier transforms in polar coordinates. In P. W. Hawkes (Ed.), *Advances in imaging and electron physics* (Vol. 165, pp. 1–45). Elsevier. https://doi.org/10.1016/B978-0-12-385861-0.00001-4

Baker, K. B., & Wing, S. (1989). A new magnetic coordinate system for conjugate studies at high latitudes. *Journal of Geophysical Research*, *94*(A7), 9139–9143. https://doi.org/10.1029/JA094iA07p09139

Basu, S., Basu, S., MacKenzie, E., Coley, W. R., Sharber, J. R., & Hoegy, W. R. (1990). Plasma structuring by the gradient drift instability at high latitudes and comparison with velocity shear driven processes. *Journal of Geophysical Research*, *95*(A6), 7799–7818. https://doi.org/10.1029/JA095iA06p07799

Boyd, T. J. M., & Sanderson, J. J. (1969). Plasma dynamics ADS bibcode. Retrieved from https://ui.adsabs.harvard.edu/abs/1969pldy.book

Bull, P., Akrami, Y., Adamek, J., Baker, T., Bellini, E., Beltrán Jiménez, J., et al. (2016). Beyond LamdaCDM: Problems, solutions, and the road ahead. *Physics of the Dark Universe*, *12*, 56–99. https://doi.org/10.1016/j.dark.2016.02.001

Buneman, O. (1963). Excitation of field aligned sound waves by electron streams. *Physical Review Letters*, *10*(7), 285–287. https://doi.org/10.1103/PhysRevLett.10.285

Canet, L., Rossetto, V., Wschebor, N., & Balarac, G. (2017). Spatiotemporal velocity-velocity correlation function in fully developed turbulence. *Physical Review E*, *95*(2), 023107. https://doi.org/10.1103/PhysRevE.95.023107

Davis, M., & Peebles, P. J. E. (1977). On the integration of the BBGKY equations for the development of strongly nonlinear clustering in an expanding universe. *The Astrophysical Journal - Supplement Series*, *34*, 425–450. https://doi.org/10.1086/190456

Dimant, Y. S., Khazanov, G. V., & Oppenheim, M. M. (2021). Effects of electron precipitation on E-region instabilities: Theoretical analysis. *Journal of Geophysical Research: Space Physics*, *126*(12), e2021JA029884. https://doi.org/10.1029/2021JA029884

Falkovich, G., Gawedzki, K., & Vergassola, M. (2001). Particles and fields in fluid turbulence. *Reviews of Modern Physics*, *73*(4), 913–975. https://doi.org/10.1103/revmodphys.73.913

Farley, D. T. (1963). A plasma instability resulting in field-aligned irregularities in the ionosphere. *Journal of Geophysical Research (1896-1977)*, *68*(22), 6083–6097. https://doi.org/10.1029/JZ068i022p06083

Farley, D. T. (1969). Incoherent scatter correlation function measurements. *Radio Science*, *4*(10), 935–953. https://doi.org/10.1029/RS004i010p00935

Farley, D. T., Ierkic, H. M., & Fejer, B. G. (1981). Radar interferometry: A new technique for studying plasma turbulence in the ionosphere. *Journal of Geophysical Research*, *86*(A3), 1467–1472. https://doi.org/10.1029/JA086iA03p01467

Fejer, B. G., & Kelley, M. C. (1980). Ionospheric irregularities. *Reviews of Geophysics*, *18*(2), 401–454. https://doi.org/10.1029/RG018i002p00401
Fredricks, R. W., & Coroniti, F. V. (1976). Ambiguities in the deduction of rest frame fluctuation spectrums from spectrums computed in moving frames. *Journal of Geophysical Research (1896-1977)*, *81*(31), 5591–5595. https://doi.org/10.1029/JA081i031p05591
Friis-Christensen, E., Lühr, H., & Hulot, G. (2006). Swarm: A constellation to study the Earth's magnetic field. *Earth Planets and Space*, *58*(4), BF03351933–358. https://doi.org/10.1186/BF03351933
Galeschuk, D. T. K. (2021). *Verification and calibration of the ICEBEAR radar through GPU acceleration, noise characterization and calculation, and radio galaxy phase calibration* (Thesis, University of Saskatchewan). Retrieved 2022-03-28, from Retrieved from https://harvest.usask.ca/handle/10388/13427 (Accepted: 2021-06-15T13:28:37Z).
Galtier, S., & Banerjee, S. (2011). Exact relation for correlation functions in compressible isothermal turbulence. *Physical Review Letters*, *107*(13), 134501. https://doi.org/10.1103/PhysRevLett.107.134501
Goodwin, L. V., & Perry, G. W. (2022). Resolving the high-latitude ionospheric irregularity spectra using multi-point incoherent scatter radar measurements. *Radio Science*, *57*(9), e2022RS007475. https://doi.org/10.1029/2022RS007475
Guizar-Sicairos, M., & Gutiérrez-Vega, J. C. (2004). Computation of quasi-discrete Hankel transforms of integer order for propagating optical wave fields. *JOSA A*, *21*(1), 53–58. https://doi.org/10.1364/JOSAA.21.000053
Hagfors, T. (1961). Density fluctuations in a plasma in a magnetic field, with applications to the ionosphere. *Journal of Geophysical Research (1896-1977)*, *66*(6), 1699–1712. https://doi.org/10.1029/JZ066i006p01699
Hong, J., Chung, J.-K., Kim, Y. H., Park, J., Kwon, H.-J., Kim, J.-H., et al. (2020). Characteristics of ionospheric irregularities using GNSS scintillation indices measured at Jang Bogo Station, Antarctica (74.62°S, 164.22°E). *Space Weather*, *18*(10), e2020SW002536. https://doi.org/10.1029/2020SW002536
Horton, W., Tajima, T., & Kamimura, T. (1987). Kelvin–Helmholtz instability and vortices in magnetized plasma. *The Physics of Fluids*, *30*(11), 3485–3495. https://doi.org/10.1063/1.866429
Huyghebaert, D., Hussey, G., Vierinen, J., McWilliams, K., & St-Maurice, J.-P. (2019). Icebear: An all-digital bistatic coded continuous-wave radar for studies of the E region of the ionosphere. *Radio Science*, *54*(4), 349–364. https://doi.org/10.1029/2018RS006747
Huyghebaert, D., St.-Maurice, J.-P., McWilliams, K., Hussey, G., Howarth, A. D., Rutledge, P., & Erion, S. (2021). The properties of ICEBEAR E-region coherent radar echoes in the presence of near infrared auroral emissions, as measured by the swarm-E fast auroral imager. *Journal of Geophysical Research: Space Physics*, *126*(12), e2021JA029857. https://doi.org/10.1029/2021JA029857
Ivarsen, M. F., Park, J., Kwak, Y.-S., Jin, Y., Knudsen, D. J., & Clausen, L. B. N. (2020). Observational evidence for the role of hall conductance in Alfvén wave reflection. *Journal of Geophysical Research: Space Physics*, *125*(12), e2020JA028119. https://doi.org/10.1029/2020JA028119
Ivarsen, M. F., Bull, P., Llinares, C., & Mota, D. F. (2016). Distinguishing screening mechanisms with environment-dependent velocity statistics. *Astronomy & Astrophysics*, *595*, A40. Retrieved 2018-09-16, from http://arxiv.org/abs/1603.03072 (arXiv: 1603.03072). https://doi.org/10.1051/0004-6361/201628604
Ivarsen, M. F., Jin, Y., Spicher, A., & Clausen, L. B. N. (2019). Direct evidence for the dissipation of small-scale ionospheric plasma structures by a conductive E region. *Journal of Geophysical Research: Space Physics*, *124*(4), 2935–2942. https://doi.org/10.1029/2019JA026500
Ivarsen, M. F., Jin, Y., Spicher, A., Miloch, W., & Clausen, L. B. N. (2021). The lifetimes of plasma structures at high latitudes. *Journal of Geophysical Research: Space Physics*, *126*(2), e2020JA028117. https://doi.org/10.1029/2020JA028117
Ivarsen, M. F., St-Maurice, J.-P., Hussey, G. C., Galeschuk, D., Lozinsky, A., Pitzel, B., & McWilliams, K. A. (2023). An algorithm to separate ionospheric turbulence radar echoes from those of meteor trails in large data sets. *Journal of Geophysical Research: Space Physics*, *128*(1), e2022JA031050. https://doi.org/10.1029/2022JA031050
Ivarsen, M. F., St-Maurice, J.-P., Jin, Y., Park, J., Miloch, W., Spicher, A., et al. (2021). Steepening plasma density spectra in the ionosphere: The crucial role played by a strong E-region. *Journal of Geophysical Research: Space Physics*, *126*(8), e2021JA029401. https://doi.org/10.1029/2021JA029401
Kelley, M. C., & Heelis, R. A. (1989). *The earth's ionosphere: Plasma physics and Electrodynamics (Chapters 1 and 3)*. San Diego: Academic Press.
Kerscher, M., Szapudi, I., & Szalay, A. S. (2000). A comparison of estimators for the two-point correlation function. *The Astrophysical Journal*, *535*(1), L13–L16. https://doi.org/10.1086/312702
Keskinen, M. J., & Huba, J. D. (1990). Nonlinear evolution of high-latitude ionospheric interchange instabilities with scale-size-dependent magnetospheric coupling. *Journal of Geophysical Research*, *95*(A9), 15157–15166. https://doi.org/10.1029/JA095iA09p15157
Keskinen, M. J., Mitchell, H. G., Fedder, J. A., Satyanarayana, P., & Zalesak, S. T. (1988). *Nonlinear evolution of the Kelvin-Helmholtz instability in the high latitude ionosphere. (Tech. Rep. No. NRL-MR-6043)*. Naval Research Lab Washington DC. Retrieved 2018-08-07, from. https://doi.org/10.1029/ja093ia01p00137 Retrieved from http://www.dtic.mil/docs/citations/ADA188875
Kintner, P. M., Ledvina, B. M., & De Paula, E. R. (2007). GPS and ionospheric scintillations. *Space Weather*, *5*(9), a–n. https://doi.org/10.1029/2006SW000260
Kintner, P. M., & Seyler, C. E. (1985). The status of observations and theory of high latitude ionospheric and magnetospheric plasma turbulence. *Space Science Reviews*, *41*(1–2), 91–129. https://doi.org/10.1007/BF00241347
Kivanç, Ö., & Heelis, R. A. (1998). Spatial distribution of ionospheric plasma and field structures in the high-latitude F region. *Journal of Geophysical Research*, *103*(A4), 6955–6968. https://doi.org/10.1029/97JA03237
Kolmogorov, A. (1941). The local structure of turbulence in incompressible viscous fluid for very large Reynolds' numbers. *Akademiia Nauk SSSR Doklady*, *30*, 301–305.
Kudeki, E., Farley, D. T., & Fejer, B. G. (1982). Long wavelength irregularities in the equatorial electrojet. *Geophysical Research Letters*, *9*(6), 684–687. https://doi.org/10.1029/GL009i006p00684
Lamarche, L. J., Deshpande, K. B., & Zettergren, M. D. (2022). Observations and modeling of scintillation in the vicinity of a polar cap patch. *Journal of Space Weather and Space Climate*, *12*, 27. https://doi.org/10.1051/swsc/2022023new
Landy, S. D., & Szalay, A. S. (1993). Bias and variance of angular correlation functions. *The Astrophysical Journal*, *412*, 64. https://doi.org/10.1086/172900
Laundal, K. M., Hatch, S. M., & Moretto, T. (2019). Magnetic effects of plasma pressure gradients in the upper F region Geophysical Research Letters. *Geophysical Research Letters*, *0*(0), 2355–2363. https://doi.org/10.1029/2019GL081980
Lisa, M. A., Gelbke, C. K., Bauer, W., Decowski, P., Gong, W. G., Gualtieri, E., et al. (1993). Impact-parameter-selected two-proton intensity interferometry for 36Ar+45Sc at E/A=80 MeV. *Physical Review Letters*, *70*(24), 3709–3712. https://doi.org/10.1103/PhysRevLett.70.3709
Lozinsky, A., Hussey, G., McWilliams, K., Huyghebaert, D., & Galeschuk, D. (2022). ICEBEAR-3D: A low elevation imaging radar using a non-uniform coplanar receiver array for E region observations. *Radio Science*, *57*(3), e2021RS007358. https://doi.org/10.1029/2021RS007358
Maynard, N. C., Bahnsen, A., Christophersen, P., Egeland, A., & Lundin, R. (1973). An example of anticorrelation of auroral particles and electric fields. *Journal of Geophysical Research*, *78*(19), 3976–3980. https://doi.org/10.1029/JA078i019p03976

Milla, M. A., & Kudeki, E. (2011). Incoherent scatter spectral theories—Part II: Modeling the spectrum for modes propagating perpendicular to B. *IEEE Transactions on Geoscience and Remote Sensing*, *49*(1), 329–345. https://doi.org/10.1109/TGRS.2010.2057253

Mounir, H., Berthelier, A., Cerisier, J. C., Lagoutte, D., & Beghin, C. (1991). The small-scale turbulent structure of the high latitude ionosphere - Arcad-Aureol-3 observations. *Annales Geophysicae*, *9*, 725–737.

Ochi, M. K. (1998). Spectral analysis. In M. K. Ochi (Ed.), *Ocean waves: The stochastic approach* (pp. 13–57). Cambridge University Press. https://doi.org/10.1017/CBO9780511529559.003

Osman, K. T., & Horbury, T. S. (2006). Multispacecraft measurement of anisotropic correlation functions in solar wind turbulence. *The Astrophysical Journal*, *654*(1), L103–L106. https://doi.org/10.1086/510906

Osman, K. T., & Horbury, T. S. (2009). Quantitative estimates of the slab and 2-D power in solar wind turbulence using multispacecraft data. *Journal of Geophysical Research*, *114*(A6). https://doi.org/10.1029/2008JA014036

Park, J., Lühr, H., Knudsen, D. J., Burchill, J. K., & Kwak, Y.-S. (2017). Alfvén waves in the auroral region, their Poynting flux, and reflection coefficient as estimated from Swarm observations. *Journal of Geophysical Research: Space Physics*, *122*(2), 2345–2360. https://doi.org/10.1002/2016JA023527

Phelps, A. D. R., & Sagalyn, R. C. (1976). Plasma density irregularities in the high-latitude top side ionosphere. *Journal of Geophysical Research*, *81*(4), 515–523. https://doi.org/10.1029/JA081i004p00515

Prikryl, P., Jayachandran, P. T., Chadwick, R., & Kelly, T. D. (2015). Climatology of GPS phase scintillation at northern high latitudes for the period from 2008 to 2013. *Annals of Geophysics*, *33*(5), 531–545. https://doi.org/10.5194/angeo-33-531-2015

Šafránková, J., Němeček, Z., Němec, F., Přech, L., Pitňa, A., Chen, C. H. K., & Zastenker, G. N. (2015). Solar wind density spectra around the ion spectral break. *The Astrophysical Journal*, *803*(2), 107. https://doi.org/10.1088/0004-637X/803/2/107

Shore, S. N., & Trimble, V. (2003). Dark matter in the universe. In R. A. Meyers (Ed.), *Encyclopedia of physical science and technology* (3rd ed., pp. 191–211). Academic Press. https://doi.org/10.1016/B0-12-227410-5/00162-9

Spicher, A., LaBelle, J., Bonnell, J. W., Roglans, R., Moser, C., Fuselier, S. A., et al. (2022). Interferometric study of ionospheric plasma irregularities in regions of phase scintillations and HF backscatter. *Geophysical Research Letters*, *49*(12), e2021GL097013. https://doi.org/10.1029/2021GL097013

Spicher, A., Miloch, W. J., & Moen, J. I. (2014). Direct evidence of double-slope power spectra in the high-latitude ionospheric plasma. *Geophysical Research Letters*, *41*(5), 1406–1412. https://doi.org/10.1002/2014GL059214

St.-Maurice, J. P., Prikryl, P., Danskin, D. W., Hamza, A. M., Sofko, G. J., Koehler, J. A., et al. (1994). On the origin of narrow non-ion-acoustic coherent radar spectra in the high-latitude E region. *Journal of Geophysical Research*, *99*(A4), 6447–6474. https://doi.org/10.1029/93JA02353

Szapudi, I., Pan, J., Prunet, S., & Budavári, T. (2005). Fast edge-corrected measurement of the two-point correlation function and the power spectrum. *The Astrophysical Journal*, *631*(1), L1–L4. https://doi.org/10.1086/496971

Tsunoda, R. T. (1988). High-latitude F region irregularities: A review and synthesis. *Reviews of Geophysics*, *26*(4), 719–760. https://doi.org/10.1029/RG026i004p00719

Verde, G., Chbihi, A., Ghetti, R., & Helgesson, J. (2006). Correlations and characterization of emitting sources. *The European Physical Journal A*, *30*(1), 81–108. https://doi.org/10.1140/epja/i2006-10109-6

Villain, J. P., Hanuise, C., & Beghin, C. (1986). ARCAD3-SAFARI coordinated study of auroral and polar F-region ionospheric irregularities. *Annales Geophysicae*, *4*, 61–68.

Welch, P. (1967). The use of fast Fourier transform for the estimation of power spectra: A method based on time averaging over short, modified periodograms. *IEEE Transactions on Audio and Electroacoustics*, *15*(2), 70–73. https://doi.org/10.1109/TAU.1967.1161901

Yeh, K. C., & Liu, C.-H. (1982). Radio wave scintillations in the ionosphere. *IEEE Proceedings*, *70*(4), 324–360. https://doi.org/10.1109/proc.1982.12313